Organic tandem solar cells

Bahro, Daniel; Wilck, Manfred; Mertens, Adrian; Ebenhoch, Bernd; von Hauff, Elizabeth; Colsmann, Alexander

published in
Progress in Photovoltaics: Research and Applications
2018

DOI (link to publisher)
10.1002/pip.3015

document version
Publisher's PDF, also known as Version of record

Received: 3 January 2018 | Revised: 12 March 2018 | Accepted: 19 March 2018

DOI: 10.1002/pip.3015

RESEARCH ARTICLE

WILEY PROGRESS IN PHOTOVOLTAICS

Organic tandem solar cells: How impedance analyses can improve the quality of external quantum efficiency measurements

Daniel Bahro[1,2] | Manfred Wilck[1] | Adrian Mertens[1] | Bernd Ebenhoch[1,2] | Elizabeth von Hauff[3] | Alexander Colsmann[1,2]

[1] Karlsruhe Institute of Technology (KIT), Light Technology Institute, Engesserstrasse 13, Karlsruhe 76131, Germany

[2] Karlsruhe Institute of Technology (KIT), Material Research Center for Energy Systems (MZE), Strasse am Forum 7, Karlsruhe 76131, Germany

[3] Vrije Universiteit Amsterdam, Department of Physics and Astronomy, De Boelelaan 1081, Amsterdam 1081 HV, The Netherlands

Correspondence
Alexander Colsmann, Karlsruhe Institute of Technology (KIT), Light Technology Institute, Engesserstrasse 13, Karlsruhe 76131, Germany.
Email: alexander.colsmann@kit.edu

Funding information
German Federal Ministry of Education and Research (BMBF), Grant/Award Number: 03EK3504

Abstract

Tandem architectures are one of the most promising concepts towards superior power conversion efficiencies of organic solar cells. An accurate determination of the power conversion efficiency requires correction of the spectral mismatch and thus relies on accurate external quantum efficiency (EQE) spectra. Due to the series connection of 2 subcells in the tandem architecture, the EQE of the tandem solar cell reproduces the EQE of one subcell if an appropriate bias light is chosen to selectively illuminate and hence forward bias the other subcell. The resulting internal voltage drop is then compensated by applying an external voltage to the tandem solar cell. In this work, we use impedance spectroscopy to accurately predict the minimum bias light intensity and the external voltage to enable accurate EQE measurements on both subcells. We exemplify this procedure on organic tandem solar cells comprising spectrally complementary absorbers and suggest an extended protocol for future measurements of the EQE.

KEYWORDS

bias illumination, bias voltage, EQE, impedance spectroscopy, organic photovoltaics, tandem solar cell

1 | INTRODUCTION

The power conversion efficiency (PCE) is an important attribute of new photovoltaic technologies and solar cell device architectures. Yet, especially in the field of organic photovoltaics, publications frequently call attention to the large number of insufficiently reported PCE data of single-junction and tandem solar cells.[1,2]

To achieve reliable results, various organizations have defined standard measurement protocols, including the definition of reference solar spectra for sample illumination. Today, the most established spectrum for PCE measurements corresponds to a standard air mass 1.5 (AM1.5) irradiation and is defined by ASTM International in the tables G173.[3] Since the spectra of test light sources never match this standard irradiation perfectly, their spectral mismatch has to be taken into account. To accurately determine the photocurrent and the PCE of solar cells, the wavelength-dependent external quantum efficiency (EQE) has to be measured to calculate the corresponding spectral mismatch factor and to compensate for this spectral mismatch.

For single-junction solar cells, measuring the EQE is rather simple and can be accomplished following established procedures such as the ASTM E1021 standard,[4] ie, by recording the wavelength-dependent short-circuit current density generated by chopped monochromatic probe light. Using a monitoring system, the illumination intensity is determined simultaneously to calculate the EQE. For higher precision, a constant bias illumination can be applied to operate the device under the desired working conditions. This is of particular importance for organic photovoltaic devices, since the magnitude of their EQE commonly depends on the applied illumination intensity.[5,6] To separate the current generated by the probe light from the current generated by the bias light, a lock-in amplifier is used for signal

recording. The lock-in amplifier removes the offset current generated from the constant bias illumination and amplifies the current generated by the chopped probe light, the latter reflecting the device's spectral response, which is then used to calculate the EQE.

For tandem solar cells, this measurement procedure has to be modified in order to obtain the specific contribution of each of the serially connected subcells. More precisely, for an accurate determination of the spectral mismatch factor, the exact EQE of each of the 2 subcells has to be measured. In the presence of a conductive intermediate contact between both subcells, the EQE of each subcell can be measured independently and the method described above can be applied.[7] For all other tandem devices without an intermediate contact, the effect of an optical bias providing spectrally selective illumination can be exploited. If a bias illumination spectrum is chosen such that one of the subcells generates a charge carrier excess (optically biased subcell), the EQE of the tandem device approaches the EQE of the second, current-limiting subcell. This method has been well established for inorganic multijunction solar cells based on compound semiconductors or amorphous silicon.[8,9] But also for new thin-film technologies such as organic photovoltaics[10] or hybrid photovoltaics,[11] this method has become the standard procedure for EQE measurements of tandem subcells.[12]

However, when applying a selective bias illumination to a tandem solar cell, the working points of both subcells differ. Following Kirchhoff's law, the same current flows through both serially connected subcells, but their voltages are different. Under selective bias illumination, the optically biased subcell produces an internal forward voltage V_{bias} close to its open-circuit voltage V_{oc}, which, if the tandem solar cell is operated at short circuit (V_{tan} = 0 V), induces a negative internal potential drop $V_{int} = -V_{bias}$ of the same magnitude across the current-limiting subcell ($V_{tan} = V_{bias} + V_{int}$). Consequently, the EQE of the current-limiting subcell is measured under reverse bias, rather than under short-circuit conditions as required by the measurement protocol. In the case of a low shunt resistance or any other reverse conductivity of the current-limiting subcell, as often observed in organic solar cells, this reverse bias leads to an overestimation of the EQE. To yield the correct EQE, an external voltage $V_{tan} = V_{bias}$ has to be applied to the tandem solar cell in order to compensate the internal voltage V_{int} across the current-limiting subcell.[10,12]

Although the necessity to apply an external voltage equal to V_{bias} is well-known and understood, an accurate estimation of V_{bias} is rather complex, and various methods have been used for its determination.[7,10] In general, V_{bias} is expected between 0 V and the V_{oc} of the optically biased subcell. Practically, its exact magnitude is inaccessible unless an intermediate contact allows its direct measurement. The voltage over the tandem device does not allow conclusions about the specific voltage distribution between the subcells. For organic tandem solar cells, Gilot et al reported a method to estimate V_{bias} based on single-junction reference devices and optical simulations, the latter requiring detailed knowledge of the optical material properties.[10] But often these efforts are omitted and either no bias voltage,[13-16] the V_{oc} of the optically biased subcell under AM1.5 illumination (as recommended by ASTM International),[12,17-19] or an arbitrary bias voltage[20] is applied. For solar cells comprising (inorganic) crystalline semiconductors, which mostly exhibit good current saturation under reverse bias, the introduced measurement errors are negligible and often do not influence the resulting EQEs significantly. But for organic tandem solar cells, applying an improper external voltage $V_{tan} \neq V_{bias}$ can lead to significant changes of the subcell EQEs and the resulting current densities.[10]

Besides an accurate estimation of V_{bias}, the selective bias light wavelength and intensity must be chosen carefully. For thin-film photovoltaics, this choice is rather complex as the optical field distribution is dominated by thin-film interferences. Especially, if spectral regimes exist where both subcells absorb, the bias illumination spectrum and intensity must be chosen very carefully.[7] The following method has been established and is commonly deployed in EQE measurements[12]: A selective bias illumination with a suitable spectral distribution is applied, and the tandem EQE is measured for increasing bias intensity. The EQE spectral shape depends on the bias intensity. At some threshold intensity, the shape of the EQE no longer changes with increasing illumination intensity and the measured EQE is considered equal to the EQE of the current-limiting subcell.[10] In most cases, this procedure yields very reliable and reproducible results.[2,10,12] However, the saturation of the tandem EQE competes with other illumination intensity dependent effects. Especially in organic solar cells, the influence of illumination-dependent charge carrier dynamics cannot be neglected.[5,6] As a consequence, the measured EQE may decrease for high illumination intensities. This can complicate the observation of the tandem EQE saturation.

The choice of the selective bias light intensity as well as the choice of the required bias voltage are important as they influence the accuracy of the subcell EQE measurements and thus the determination of the tandem solar cell efficiency. Hence, in particular for organic tandem solar cells, new methods are required to either improve or replace the procedures used so far.

In this work, we suggest a new method to accurately measure the subcell EQE spectra in organic tandem solar cells: Using impedance spectroscopy, we find excellent predictions for the selective bias illumination intensity and for the external voltage to be applied to the tandem solar cell during the EQE measurement.

2 | SUBCELL VOLTAGE SATURATION IN TANDEM SOLAR CELLS

For a specific tandem solar cell, V_{bias} is inherently linked to the selective bias light spectrum and intensity.[21] The spectrum of the bias light affects, depending on the EQE of the subcells, the required bias illumination intensity. Furthermore, it influences V_{bias}, which is introduced by the optically biased subcell. To illustrate this complex interplay, we studied the subcell voltages in more detail. Specifically, we determined V_{bias} while increasing the intensity of the selective bias illumination until saturation was observed.

Direct measurement of the subcell voltages is impossible in a serially connected tandem solar cell since only the 2 outer contacts are available. Therefore, in addition to the 2-terminal tandem solar cells studied herein, we also build 3-terminal tandem solar cell proxies comprising a third intermediate contact according to a previously published procedure.[7] The 3-terminal proxy devices exhibit the same

optoelectronic properties as the 2-terminal tandem solar cells but enable direct access to the individual subcell voltages and facilitate the interpretation of the impedance measurements on tandem solar cells discussed later in this work.

The tandem device architecture and the corresponding layer thicknesses of the 3-terminal devices are depicted in Figure 1 A. All tandem solar cells studied herein consist of absorber layers comprising poly[[4,8-bis[(2-ethylhexyl)oxy]benzo[1,2-*b*:4,5-*b*′] dithiophene-2,6-diyl][3-fluoro-2-[(2-ethylhexyl)carbonyl]thieno[3,4-*b*] thiophenediyl]] and [6,6]-phenyl C_{71}-butyric acid methyl ester (PTB7:$PC_{71}BM$) in the bottom subcell as well as poly[2,7-(5,5-bis-(3,7-dimethyloctyl)-5H-dithieno[3,2-*b*:2′,3′-*d*]pyran)-*alt*-4,7-(5,6-difluoro-2,1,3-benzothiadiazole)] and [6,6]-phenyl C_{61}-butyric acid methyl ester (PDTP-DFBT:$PC_{61}BM$) in the top subcell as reported in an earlier publication.[22] The third intermediate contact is fabricated from conductive poly[3,4-ethylenedioxythiophene]:poly[4-styrenesulfonate] (c-PEDOT:PSS) and is incorporated into the recombination zone, which is made of m-PEDOT:PSS (modified by additional sodium polystyrene sulfonate) and zinc oxide. By choosing the total thickness of the c-PEDOT:PSS and m-PEDOT:PSS bilayer of the 3-terminal tandem solar cells equal to the thickness of the m-PEDOT:PSS layer of the tandem solar cells without intermediate contact, identical optical properties are obtained. Thus, the third intermediate contact does not change the optical field distribution within the tandem solar cells.[7] The intermediate c-PEDOT:PSS contact allows the direct measurement of the individual current density–voltage (*J-V*) curves of both subcells (Figure 1B).

The PTB7:$PC_{71}BM$ and PDTP-DFBT:$PC_{61}BM$ subcells not only exhibit spectrally complementary absorption but also cover a broad spectral regime between 300 and 750 nm where both absorbers compete for photon harvesting. The extended absorption of PDTP-DFBT:$PC_{61}BM$ into the infrared allows to selectively excite the top subcell with a 780-nm LED bias light illumination. Under this 780-nm bias light illumination, the PDTP-DFBT:$PC_{61}BM$ top subcell generates a significant photocurrent whereas the PTB7:$PC_{71}BM$ bottom subcell responds only weakly. As a consequence, the PTB7:$PC_{71}BM$ bottom subcell is reverse biased by V_{int}. To drive the current-limiting bottom subcell into short-circuit conditions as required for EQE measurements, V_{int} has to be compensated. Figure 1B depicts the *J-V* curves of the tandem device and its subcells under illumination (780 nm, 1 mW cm^{-2}). According to Kirchhoff's law, the required external voltage $V_{tan} = V_{bias} = 0.63$ V to compensate V_{int} can be determined from the intersection of the *J-V* curves of the optically biased top subcell and the tandem *J-V* curve. V_{bias} strongly depends on the bias light intensity: At zero intensity (in the dark), we find $V_{bias} = 0$ V. The change of V_{bias} upon increasing the intensity from 0.25 to 5 mW cm^{-2} is indicated by the black arrow in Figure 1B. Towards higher selective bias light intensities, V_{bias} approaches the V_{oc} of the optically biased subcell. This process becomes clear in Figure 1C, which depicts V_{bias} as well as the ratio of V_{bias} and the V_{oc} as a function of the applied bias light intensity from the 780-nm LED. At around 3 mW cm^{-2}, we found a constant V_{bias}/V_{oc}, which reflects the saturation of V_{bias}. In accordance with prior reports, we henceforth refer to the constant V_{bias}/V_{oc} as subcell voltage saturation. In absolute numbers, V_{bias} and V_{oc} do not saturate but rather show logarithmic dependence on the illumination intensity. Again, we note that in tandem solar cells without intermediate contact, the V_{oc} of the subcells cannot be measured directly. The smaller the slope of V_{bias} versus bias light intensity, the smaller is the change in the measured EQE. Hence, for a saturated V_{bias}, the measured EQE of the tandem solar cell reproduces the EQE of the current-limiting subcell. Figure 1C shows that the largest changes in V_{bias} occur below 3 mW cm^{-2} whereas, for higher bias illumination intensities, V_{bias} saturates. We conclude that, to measure the bottom subcell EQE using the 780 nm LED bias illumination, here, a bias light intensity of at least 3 mW cm^{-2} is required.

Having access to the subcell voltage saturation curve through an intermediate contact enables a much more careful choice of the bias light, its intensity, and the resulting bias voltage and hence improves the accuracy of the subcell EQE measurement. Unfortunately, this curve is inaccessible for tandem solar cells in the much more common 2-terminal configuration. Therefore, in the following, we present a method to reconstruct the described voltage saturation from impedance data of the tandem solar cells without direct access to their subcells.

3 | IMPEDANCE SPECTROSCOPY

Impedance spectroscopy is a well-established method in solar cell research. Commonly, it is used to reveal charge carrier processes in bulk materials and at interfaces.[23] The device architectures are kept

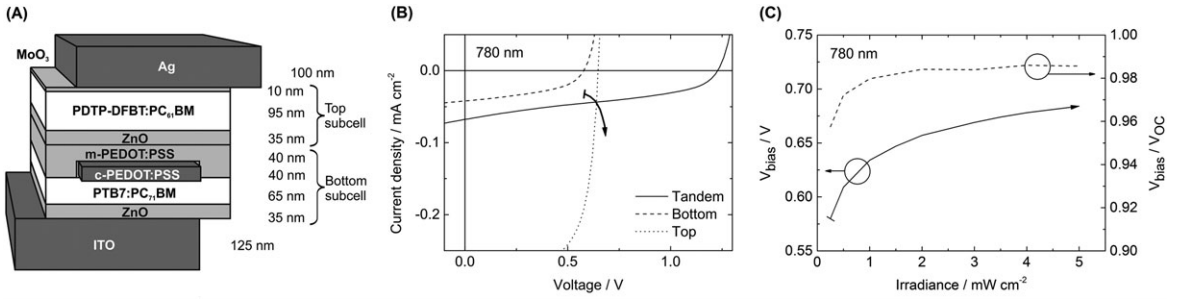

FIGURE 1 A, Device architecture and layer thicknesses of the 3-terminal tandem solar cell. B, Current density-voltage (*J-V*) curves of the tandem device and its subcells under 780-nm LED bias illumination. The optically biased PDTP-DFBT:$PC_{61}BM$ subcell (top solar cell) delivers a much higher current density than the current-limiting PTB7:$PC_{71}BM$ subcell (bottom solar cell). The required external voltage $V_{tan} = V_{bias}$ can be determined from the intersection of the *J-V* curves of the tandem device and the optically biased subcell. The arrow represents the evolution of V_{bias} towards higher bias light illumination intensity. C, V_{bias} and V_{bias}/V_{oc} as a function of the bias light intensity

simple to easily distinguish between different internal processes. Commonly, equivalent circuit models are designed for and fitted to the experimental data. By interpreting individual components of the model and by correlating these components to physical processes, conclusions about charge carrier dynamics, such as transport and recombination, are drawn.

Tandem solar cells inherently consist of complex multilayer architectures. The corresponding models would be rather extensive and comprise many components, rendering the assignment of certain model components to specific interfaces or layers almost impossible. Inaccuracies can arise if the chosen model fails to perfectly reproduce the experimental data. That is why, so far, only a single report discusses impedance data of organic tandem solar cells.[24]

Due to the complexity of tandem solar cells, we have chosen a different approach to interpret the impedance spectroscopy data. Instead of generating a model to describe our devices, we analyze the experimental data graphically. This analysis can be applied independently of the device architectures and materials used. In the following section, we provide the mathematical basis for our graphical analysis of impedance data.

3.1 | Complex impedance data

First, to gain a better understanding of the observed impedance response of organic tandem solar cells, a very basic model is used. We approximate the impedance Z of an organic single-junction solar cell by an equivalent circuit consisting of a parallel connection of a capacitance C and a resistance R.[25] This model is different from the equivalent circuit consisting of two RC elements that is more often used in the literature,[26,27] but it is sufficient for modelling the features observed later. We note that interface effects, space charge regions or severe charge carrier trapping can alter the impedance data and may lead to multiple RC elements. If present, such multiple RC elements require an advanced analysis. A single relaxation is expressed by Equation 1 with the characteristic frequency ω_c in Equation 2:

$$Z = \frac{R}{1 + j\,\omega RC}, \tag{1}$$

$$\omega_c = \frac{1}{RC}, \tag{2}$$

where j is the imaginary unit and ω the angular frequency. It is well accepted that R is linked to recombination processes and therefore depends on the illumination intensity and the applied voltage. The series resistance of the electrodes is neglected. Hence, according to Equation 2, ω_c also depends on the applied illumination intensity and voltage. The capacitance C results from the sum of the geometric capacitance C_g and the chemical capacitance C_μ.[28] Whereas C_g can be considered constant, C_μ reflects the charge carrier storage capability depending on the energetic alignment and increases when approaching flat band conditions.[29] Under high reverse bias, C_μ becomes negligible, which allows the direct measurement of C_g.

This model leads to the typical semicircles with a diameter equal to R in Cole-Cole impedance plots where the imaginary part Z'' is plotted as a function of the real part Z'.[30] The Cole-Cole plots of PDTP-DFBT:$PC_{61}BM$ single-junction solar cells under 780-nm LED illumination in Figure 2A,B illustrate the effect of the voltage and the illumination intensity applied during the impedance measurement on the diameter of the semicircles. Since both, voltage and illumination intensity, simultaneously affect R, the graphical interpretation of the impedance data may yield ambiguous results. For better access to voltage changes without fitting the data to a specific model, a different illumination-independent representation of the measured data is required.

3.2 | Electric modulus

The electric modulus M was introduced by McCrum et al and used by Glatthaar et al to describe organic solar cells[31,32]:

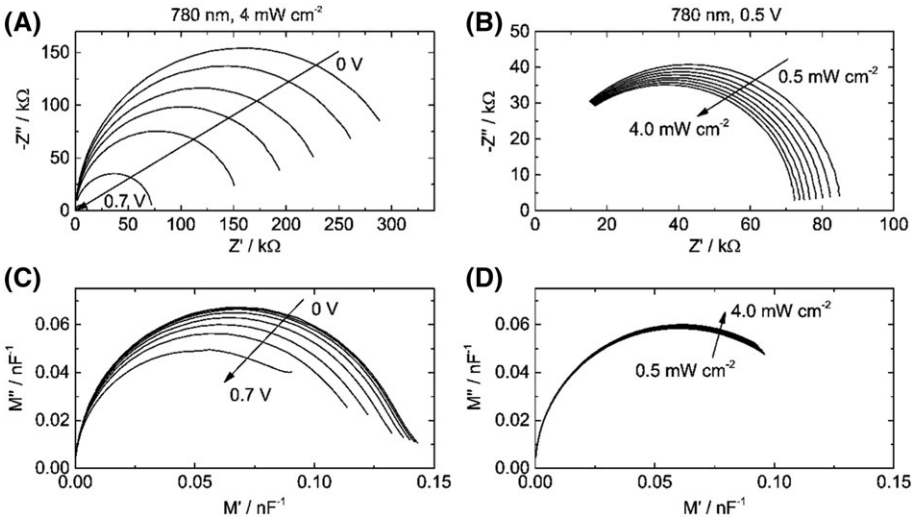

FIGURE 2 A, Cole-Cole plot of the impedance data gathered from a PDTP-DFBT:$PC_{61}BM$ single-junction solar cell under 780-nm bias light illumination. Increasing the applied voltage (0 to 0.7 V, step-width 0.1 V) reduces the diameter of the semicircles. B, The illumination intensity (0.5 to 4 mW cm^{-2}, step-width 0.5 mW cm^{-2}) also affects the semicircles' diameters. C and D, The diameter of the semicircles of the electric modulus plots of the same data are only sensitive to the applied voltage but not to the bias light illumination intensity

$$M = j\omega C_0 Z. \tag{3}$$

The geometric capacitance of an empty solar cell C_0 (permittivity equals 1) cannot be measured directly. To later enable comparison of tandem and reference solar cells with potentially different photoactive layer thicknesses, we refrain from calculating C_0 using the equation for a simple capacitor but set C_0 to unity. Consequently, M is expressed in units of F^{-1}. Using Equation 1, the electric modulus of an organic solar cell can be expressed by Equation 4:

$$M = \frac{j\omega R}{1 + j\,\omega RC}. \tag{4}$$

Plotting the electric modulus data in a Cole-Cole diagram (imaginary part M'' versus real part M') results in a semicircle with a diameter of $\frac{1}{C}$ centered at $\frac{1}{2C}$ (Equation 5). For increasing angular frequencies ω, the data points shift from 0 to $\frac{1}{C}$ according to Equations 6 and 7.

$$\left|\frac{1}{2C} - M\right| = \frac{1}{2C}, \tag{5}$$

$$\lim_{\omega \to 0} M = 0, \tag{6}$$

$$\lim_{\omega \to \infty} M = \frac{1}{C}. \tag{7}$$

From the impedance plots in Figure 2A,B, we calculate the electric modulus plots depicted in Figure 2C,D. The semicircle's diameter now corresponds to $\frac{1}{C}$. The dependency of the diameter on the applied voltage is shown in Figure 2C. The illumination intensity in Figure 2 D, however, shows only negligible influence on the semicircle's diameter since the capacitance itself can be considered independent of the illumination intensity. Hence, omitting any modelling, the electric modulus plots allow us to distinctly investigate the influence of the applied voltage while being decoupled from the influence of the illumination intensity.

3.3 | Impedance spectroscopy on tandem solar cells

Next, we applied the method described above to organic tandem solar cells in 2-terminal configuration, without a third intermediate contact (Figure 3A). When characterizing tandem solar cells by impedance spectroscopy, 2 features resulting from the 2 subcells are expected (see Figure S2). Depending on the characteristic frequency $\omega_{c,1}$ and $\omega_{c,2}$ of the individual subcells, these features can be clearly separated or, if $\omega_{c,1}$ and $\omega_{c,2}$ of both subcells are equal, can merge into one curve, which cannot be distinguished from a single-junction solar cell. Under very selective illumination by appropriate bias light as discussed herein, $\omega_{c,1}$ and $\omega_{c,2}$ exhibit very different magnitudes which allows to identify the contributions of each subcell.

Figure 3B shows a Cole-Cole impedance plot of the tandem solar cell, which is illuminated by a 780-nm LED (bias) light source. The PDTP-DFBT:PC_{61}BM absorber layer shows very strong absorption at 780 nm and hence is optically biased, whereas the PTB7:PC_{71}BM

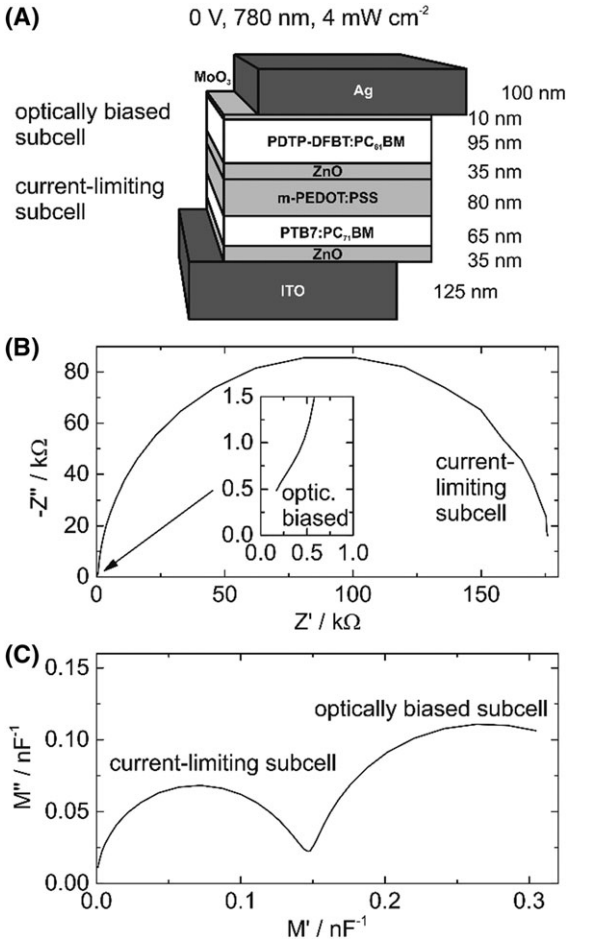

FIGURE 3 A, Two-terminal tandem solar cell architecture without a third intermediate contact. The top subcell is optically biased (4 mW cm^{-2}, 780 nm) and the bottom subcell limits the device current. B, In Cole-Cole impedance plots, the semicircle diameters of both subcells appear on different impedance scales, and hence, the semicircles are difficult to distinguish. C, Plotting the same data in an electric modulus plot results in 2 clearly distinguishable semicircles

absorber layer responses only weakly to this illumination and hence is current limiting. The selective absorption leads to very different magnitudes of R for both subcells (PTB7:PC_{71}BM subcell: 175 kΩ and PDTP-DFBT:PC_{61}BM subcell: 660 Ω) and hence to two separated semicircles in the impedance plot (Figure 3B). While the data of the current-limiting subcell strongly dominates the graph, the contribution of the optically biased subcell almost vanishes and cannot clearly be identified as semicircle (Figure 3B, inset). The latter may also originate from charge carrier transport or other effects.[33-35]

In contrast, the electric modulus plot of the same data in Figure 3C shows 2 clearly separated semicircles. Notably, the transformation to the electric modulus plot (Equation 3) does not influence the characteristic frequencies (Equation 2). Hence, as observed in impedance plots, the separation of the 2 subcell features originates from a difference in $\omega_{c,1}$ and $\omega_{c,2}$ of both subcells (PTB7:PC_{71}BM subcell: 820 s^{-1}, PDTP-DFBT:PC_{61}BM subcell: 330 × 10^3 s^{-1}). Here, the semicircles exhibit almost the same diameter, since they are related to the subcell capacitances C_1 and C_2, which are, in organic solar cells, often on the same order of magnitude. In the electric modulus plot (Figure 3C), the semicircle of the current-limiting subcell can be found

on the left side, in the low-frequency regime, due to the lower ω_c and the semicircle of the optically biased subcell on the right side in the high-frequency regime. Figure 3C clearly demonstrates the advantage of the electric modulus plots, whereas other representations, such as impedance versus frequency or capacitance versus voltage graphs, may be difficult to interpret.

Most importantly, in agreement with the observation in single-junction solar cells (Figure 2), the diameters of the individual semicircles of the tandem solar cell are directly related to the voltages across the subcells and are independent of the illumination intensity. This finding allows to study the subcell voltage changes under various illumination conditions without requiring electrical access to the individual subcells by a third intermediate contact.

4 | BIAS LIGHT INTENSITY

As described above, the subcell voltage saturation correlates with the minimum intensity of the selective bias light required to make the tandem EQE reproduce the EQE of the current-limiting subcell. To measure the EQE of the PTB7:$PC_{71}BM$ and PDTP-DFBT:$PC_{61}BM$ subcells, 2 different LED bias light sources, 780 and 627 nm, were chosen resulting in 2 completely different operation scenarios. Figure 4A,B elucidates these 2 scenarios, showing optical simulation results of the numbers of absorbed photons throughout the tandem device, taking into account the measured spectral irradiance of the respective bias light source. Under illumination with 780 nm bias light (Figure 4A), we found only a weak response from the PTB7:$PC_{71}BM$ subcell, but a strong response from the PDTP-DFBT:$PC_{61}BM$ subcell. Dominant absorption in one subcell enables good optical biasing even at low bias light intensities. In contrast, the simulation of the tandem solar cell response under 627-nm LED bias illumination shows that both subcells absorb significant amounts of photons and hence strongly compete for photon harvesting. The PTB7:$PC_{71}BM$ layer absorbs only some more photons than the PDTP-DFBT:$PC_{61}BM$ subcell. We note that, in an experimental setup, the photo current ratio would be slightly different than the ratio of absorbed photons discussed in these simulations due to the internal quantum efficiency of PTB7:$PC_{71}BM$ being higher than the internal quantum efficiency of PDTP-DFBT:$PC_{61}BM$.[36,37]

The voltage saturation curves in Figure 4C,D that were measured on the 3-terminal proxy devices confirm these theoretic predictions: Under 780-nm bias illumination, V_{bias}, generated by the PDTP-DFBT:$PC_{61}BM$ subcell, saturates above 3 mW cm^{-2} (Figure 4C). Under 627-nm bias light illumination, however, much higher intensities (>6 mW cm^{-2}) are required to reach saturation of V_{bias} of the PTB7:$PC_{71}BM$ solar cell (Figure 4D).

Since V_{bias} is inaccessible in conventional 2-terminal tandem solar cells, we performed impedance spectroscopy measurements to reveal the illumination-dependent voltage changes. Figure 4E,F depict the electric modulus plots of the 2-terminal tandem solar cell under both bias illumination scenarios. Starting from a dark measurement and moving towards higher bias light intensity, a valley develops, which divides the curve into two semicircles. Above a certain bias light illumination intensity, the valley depth remains constant. To explain this observation and to correlate this valley with the voltage saturation, we examine the ratio r_c of the characteristic frequencies $\omega_{c,1}$ and $\omega_{c,2}$ of the current-limiting and the optically biased subcell.

$$r_c = \frac{\omega_{c,1}}{\omega_{c,2}} = \frac{R_2 C_2}{R_1 C_1}, \qquad \omega_{c,1} \leq \omega_{c,2}. \tag{8}$$

If r_c equals 1, both subcells exhibit the same characteristic frequency and the electric modulus graph shows one common semicircle. If $r_c < 1$, the characteristic frequencies are different and 2 overlapping semicircles can be observed. In general, the depth of the valley between the 2 semicircles reflects the magnitude of r_c. According to Equation 8, r_c depends on R and C of both subcells (R_1, C_1 and R_2, C_2). On the one hand, as discussed above, C_1 and C_2 are illumination independent (Figure 2D) and hence changes in $\frac{C_2}{C_1}$ can only stem from voltage changes at the subcells. Thus, if the voltages across the subcells are constant, $\frac{C_2}{C_1}$ is constant. On the other hand, R depends much less on the illumination intensity than on the applied voltage (see Figure 2A,B) and the ratio $\frac{R_2}{R_1}$ can also be considered constant for constant subcell voltages within a certain illumination intensity range. Altogether, the characteristic frequency ratio r_c only depends on the voltage at both subcells. If V_{bias} saturates, the depth of the valley between the subcell curves also saturates, which is nicely reflected in the experimental electric modulus curves in Figure 4E,F. For 780-nm bias light illumination, the electric modulus curves remain unaffected under illumination intensities higher than 3.0 mW cm^{-2}. For 627-nm bias light illumination, we find a saturated electric modulus plot when the illumination intensity exceeds 6.0 mW cm^{-2}. This saturation of the electric modulus is in agreement with the voltage saturation in Figure 4C,D. Hence, from the impedance data of the tandem solar cells under different illumination intensities, the minimum bias light intensity for subcell voltage saturation can be obtained, which is also the minimum bias illumination intensity to be applied during subcell EQE measurements.

As discussed above, the voltage saturation of the optically biased subcell corresponds to a tandem EQE approaching the EQE of the current-limiting subcell. This saturation is commonly determined by measuring the tandem EQE while increasing the bias light illumination intensity until no further change in the spectral shape of the EQE is observed. Following this established protocol to measure the EQE of the 2-terminal tandem solar cells for an increasing intensity of the 780 nm bias light (Figure 4G), we found a perfect match to the observations made in the electric modulus plot (Figure 4E). Under 780-nm bias light illumination, the EQE curves exhibit no further changes for intensities beyond 3.0 mW cm^{-2}. In contrast, under 627-nm bias light illumination, no clear saturation of the EQE is observed (Figure 4H). Due to 2 competing processes that influence the EQE magnitude, the EQE curve changes further even at illumination intensities higher than 6.0 mW cm^{-2} (value predicted by the electric modulus plots). The first process is the EQE saturation, where the measured tandem EQE approaches the EQE of the current-limiting subcell. The second process is the dependency of the subcell EQE on the illumination intensity due to changing charge carrier densities and hence recombination rates. The changed charge carrier interaction leads to a decreasing EQE for increasing illumination intensities as previously observed for many organic absorber materials.[5,6] This leads to

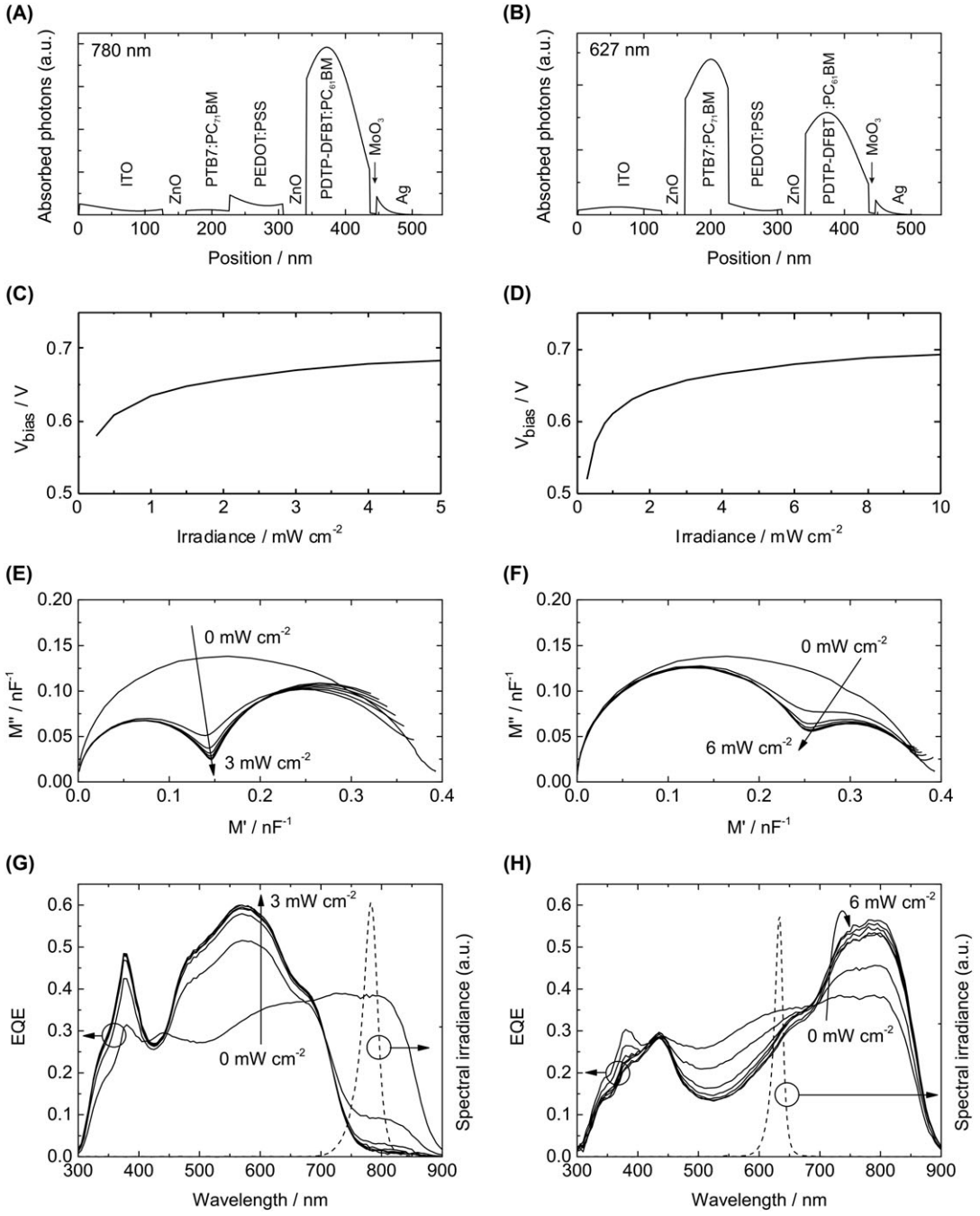

FIGURE 4 Left column: 780-nm LED bias light illumination; right column: 627-nm LED bias light illumination. A, The simulated distribution of the number of absorbed photons throughout the tandem device under 780-nm illumination shows a very selective response of the subcells. B, Under 627-nm illumination, a stronger competition for photon harvesting yields a more balanced absorption of photons in both subcells. C, V_{bias} measured on 3-terminal tandem solar cell under 780-nm bias light illumination saturates at around 3 mW cm^{-2}. D, Under 627-nm bias light illumination, saturation occurs at intensities beyond 6 mW cm^{-2}. E, Electric modulus plots under 780 nm bias illumination for different intensities (0 to 3.0 mW cm^{-2}, step-width 0.5 mW cm^{-2}). The electric modulus saturates at 3.0 mW cm^{-2}. For higher bias light illumination intensities, no further change is observed (data not shown). F, Under 627-nm bias light illumination, we observe the same dependency of the electric modulus on the bias light illumination intensity with saturation at 6.0 mW cm^{-2} (0 to 6.0 mW cm^{-2}, step-width 1.0 mW cm^{-2}). G, Towards 3.0 mW cm^{-2} bias light illumination intensity, the external quantum efficiency (EQE) of the tandem solar cell approaches the EQE of the current-limiting PTB7:$PC_{71}BM$ subcell (0 to 3.0 mW cm^{-2}, 0.5 mW cm^{-2} steps). Notably, the intensity at which the tandem EQE perfectly resembles the subcell EQE corresponds to the saturation intensity determined from the electric modulus plots measured on the 2-terminal tandem solar cells. H, The same holds true under 627 nm bias light illumination (0 to 6.0 mW cm^{-2}, 1.0 mW cm^{-2} steps). In the latter case, additional intensity-dependent effects lead to a continuous change in EQE instead of a saturation

a continuous transformation of the EQE. Here, the analysis of the voltage saturation by means of IS can lead to a better understanding of the EQE saturation. The impedance analysis can predict the bias light illumination intensity at which the tandem EQE reflects the subcell EQE. This is in particular helpful if choosing an appropriate bias light illumination is difficult due to absorption in both subcells, or if strongly

intensity dependent mechanisms induce a continuous EQE transformation towards higher bias light illumination intensities.

5 | BIAS VOLTAGE

So far, the analysis of the electric modulus plots has revealed a saturation of the subcell voltages, however, without allowing conclusions on the exact voltage drop across each subcell. As described in Section 4 and based on observing the relative voltage changes of the subcells, the minimum intensity of the selective bias illumination for measuring the subcell EQE can be obtained, but not the accurate magnitude of V_{bias}. As discussed in Section 1, an external voltage $V_{tan} = V_{bias}$ is required to compensate the voltage drop V_{int} at the current-limiting subcell, and it depends on the intensity of the selective bias illumination (Figure 1C). Applying the open-circuit voltage of the optically biased subcell under AM1.5 standard illumination is a first approximation, but, for higher accuracy, a more thorough determination of V_{bias} is inevitable.

Although the voltage change across each subcell can be observed in the electric modulus plots, for the determination of exact voltages, knowledge of the dependency of the subcell's electric modulus on the applied voltage is needed. Therefore, a reference device is required, which allows to relate the measured impedance data to a certain voltage. It needs to be characterized by the same method that is used to characterize the tandem solar cell. To design a reference device that yields the same impedance response as the corresponding subcell, 2 rules have to be obeyed: (1) All dielectric layers, ie, effectively the absorber layer, have to have the same thickness used in the tandem solar cell. Not obeying to this criterion would influence the capacitance. (2) All materials in direct contact with the dielectric layers shall not be replaced by others to avoid changes of the chemical capacitance C_μ and of the shape of the electric modulus function.

Importantly, for comparison of the impedance data of a tandem solar cell and a reference solar cell, the electric modulus must not depend on the optical field distribution. As depicted in Figure S1, from sample illumination with different spectral distributions that generate different optical field distributions in the photoactive layers, indeed, the same impedance response is obtained.

5.1 | Decoupling the subcells' impedance data

To determine the external voltage $V_{tan} = V_{bias}$ to be applied to the tandem solar cell under selective bias illumination, we measured its electric modulus. In Cole-Cole plots, both subcells produce distinct semicircles under selective illumination (dashed lines in Figure 5A,B). But whenever the valley between the subcell semicircles does not touch the M' axis, all data derived from the first semicircle are slightly influenced by contributions from the second semicircle and vice versa. So far, we neglected the overlap of both subcell semicircles, but this overlap must not be neglected when comparing the semicircles of a tandem subcell and the corresponding single-junction device, the latter not being influenced by the second subcell (see Figure S3). To eliminate this coupling between the 2 semicircles, we introduce a new transformation from the complex impedance Z to an effective electric modulus M_{eff} (Equation 9) by adding an additional effective series resistance $R_{s,eff}$.

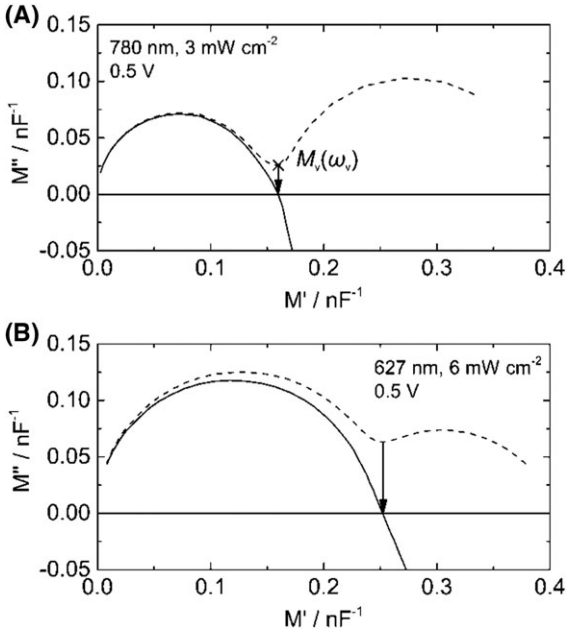

FIGURE 5 A, The electric modulus of the current-limiting subcell can be calculated using Equation 9. The effective series resistance $R_{s,eff}$ is determined from $M_v(\omega_v)$, which is extracted from the valley between the subcell semicircles. Under 780-nm LED bias light illumination, we find only a small difference between M (dashed line) and M_{eff} (solid line). B, Under 627-nm LED bias light illumination, a larger difference is observed

$$M_{eff} = j\omega C_0 \left(Z - R_{s,eff}\right). \tag{9}$$

Again, we set the geometric capacitance of the empty device C_0 to unity. We exemplify this new transformation on a single subcell using the basic model described by Equation 1. Using the impedance Z from Equation 1 for both subcells, the electric modulus of the tandem solar cell can be expressed by Equation 10:

$$M = M_1 + M_2 = \frac{j\omega R_1}{1 + j\omega R_1 C_1} + \frac{j\omega R_2}{1 + j\omega R_2 C_2}. \tag{10}$$

Here, M, M_1, and M_2 represent the electric moduli of the tandem solar cell and the 2 subcells, respectively. For all angular frequencies ω much smaller than the characteristic frequency of the optically biased subcell $\omega_{c,2}$ (see Equations 2 and 8), this model can be simplified to Equation 11:

$$M = \frac{j\omega R_1}{1 + j\omega R_1 C_1} + j\omega R_2. \tag{11}$$

Applying the effective electric modulus M_{eff} from Equation 9 with an effective series resistance $R_{s,eff}$ equal to the parallel resistance of the optically biased subcell R_2, the effective electric modulus M_{eff} becomes the electric modulus of the current-limiting subcell M_1 (Equation 12).

$$R_{s,eff} = R_2 \; M_{eff} = \frac{j\omega R_1}{1 + j\omega R_1 C_1} = M_1. \tag{12}$$

We estimate $R_{s,eff}$ from the position of the valley between the subcell semicircles. From Equation 3, we derive Equation 13 describing the real part of the impedance Z'.

$$Z' = \frac{M''}{\omega}. \quad (13)$$

Z' only depends on the imaginary part of the electric modulus M'' and the angular frequency ω. Using the imaginary part of the minimum of the valley M_v'' and the corresponding angular frequency ω_v (see Figure 5A), the effective series resistance can be calculated.

$$R_{s,\mathrm{eff}} = \frac{M_v''}{\omega_v}. \quad (14)$$

Altogether, this transformation decouples the contributions of both subcells to the impedance data and hence allows the extraction of precise subcell characteristics. For reference, we verified this procedure on the 3-terminal tandem solar cells (Figure S3).

This new formalism enables the analysis of the previously recorded impedance data of the tandem solar cells to find the correct external voltages V_{tan} required to measure the EQEs of the PDTP-DFBT:$PC_{61}BM$ and the PTB7:$PC_{71}BM$ subcells. Transforming the saturated electric modulus data of the tandem device under 780- and 627-nm bias illumination in Figure 5A,B (dashed lines), respectively, using Equation 9, we yield the effective electric moduli M_{eff} (Figure 5A,B, solid lines) that resemble the electric moduli of the respective current-limiting subcell. The valley between the former semicircles now intersects the real M' axes and all data points corresponding to the optically biased subcell become negative.

We note that, under selective 780-nm bias illumination, we observed almost no difference between M and M_{eff}, which in principle would allow to use the uncorrected data M instead of calculating M_{eff}. However, under 627-nm LED illumination, the situation is different: Both characteristic frequencies $\omega_{c,1}$ and $\omega_{c,2}$ are much closer, the coupling of the semicircles cannot be neglected, and using M_{eff} becomes mandatory.

To compare the electric modulus curve of one of the subcells to the electric modulus curve of the corresponding reference solar cell, both must exhibit the same impedance response. Therefore, we recommend comparing the geometric capacitance C_g of both solar cells first. As described above, under high reverse bias, the capacitance approaches C_g. Then the electric modulus function reflects a device with almost complete charge carrier depletion. When illuminating the tandem solar cell selectively and simultaneously applying a high reverse bias, the same depletion occurs in the current-limiting subcell. If both C_g of the current-limiting subcell and C_g of the corresponding reference device are equal, the geometries of the dielectric layers are equal. Since the reference device consists of the same materials as the tandem subcell, this leads to very similar electric modulus and proves comparability of the reference device and the subcell.

5.2 | Voltage relations in tandem solar cells

We note that, for complete voltage saturation, the voltage drop across the optically biased subcell V_{bias} is constant for a broad range of voltages applied to the tandem solar cell V_{tan} (Figure 6), since the conductivity of the optically biased subcell is much larger than the conductivity of the current-limiting subcell. The voltage introduced to the current-limiting subcell V_{int} can be calculated by $V_{int} = V_{tan} - V_{bias}$.

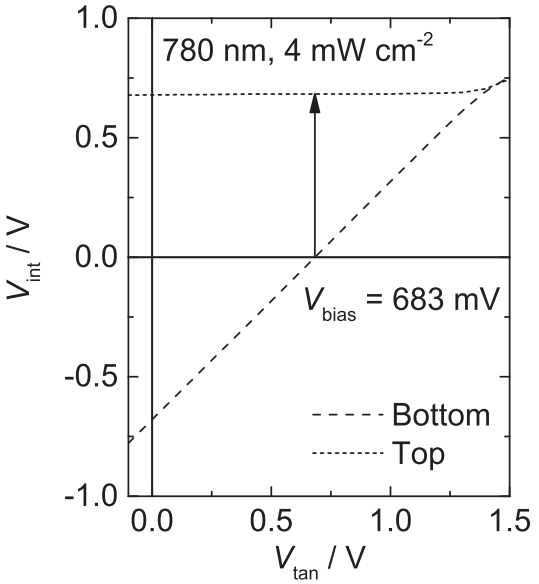

FIGURE 6 The voltage of the current-limiting subcell V_{int} as a function of the voltage applied to the tandem solar cell V_{tan}. Under sufficiently high selective bias illumination intensities, $V_{bias} = V_{tan} - V_{int}$ is constant for a broad range of V_{tan}

The constant offset between the tandem voltage V_{tan} and V_{int} allows the determination of the bias voltage V_{bias} not only at the intersection of the tandem solar cell's *J-V* curve and the *J-V* curve of the optically biased subcell but also at almost all other working points below the V_{oc} of the tandem solar cell. Hence, the accuracy of V_{bias} can be improved significantly by comparing the tandem subcell and the reference solar cell at different voltages.

5.3 | Application to PTB7:$PC_{71}BM$/PDTP-DFBT:$PC_{61}BM$ tandem solar cells

We exemplify the measurement protocol described above on the determination of the external voltages required to accurately measure the EQEs of the PDTP-DFBT:$PC_{61}BM$ and the PTB7:$PC_{71}BM$ subcells.

Obeying to the rules for building reference devices above, we fabricated the single-junction reference solar cells depicted in Figures 7A, B: For the PTB7:$PC_{71}BM$ subcell, we built ITO/ZnO/PTB7:$PC_{71}BM$/m-PEDOT:PSS/Ag and, for the PDTP-DFBT:$PC_{61}BM$ subcell, ITO/m-PEDOT:PSS/ZnO/PDTP-DFBT:$PC_{61}BM$/MoO_3/Ag reference solar cells. We assumed that the electrodes, the m-PEDOT:PSS, and the ZnO layers behave like conductors in impedance spectroscopy, and that the absorber layers behave like dielectrics. We note that, against expectations, the m-PEDOT:PSS layer in ITO/m-PEDOT:PSS/ZnO/PDTP-DFBT:$PC_{61}BM$/MoO_3/Ag solar cells is not obsolete, as we found some influence of the m-PEDOT:PSS/ZnO interface on the measured capacitance.

Here, we determined V_{bias} under the previously obtained minimum bias illumination intensities (3.0 mW cm^{-2} under 780-nm LED bias light; 6.0 mW cm^{-2} under 627 nm LED bias light; Figure 4), but the procedure would yield equally good results under higher bias light intensities. First, we recorded the electric moduli M of the tandem solar cell under selective bias illumination (780 and 627 nm) for a set of voltages (0.5 to 1.2 V, step width 0.05 V) and calculated M_{eff}

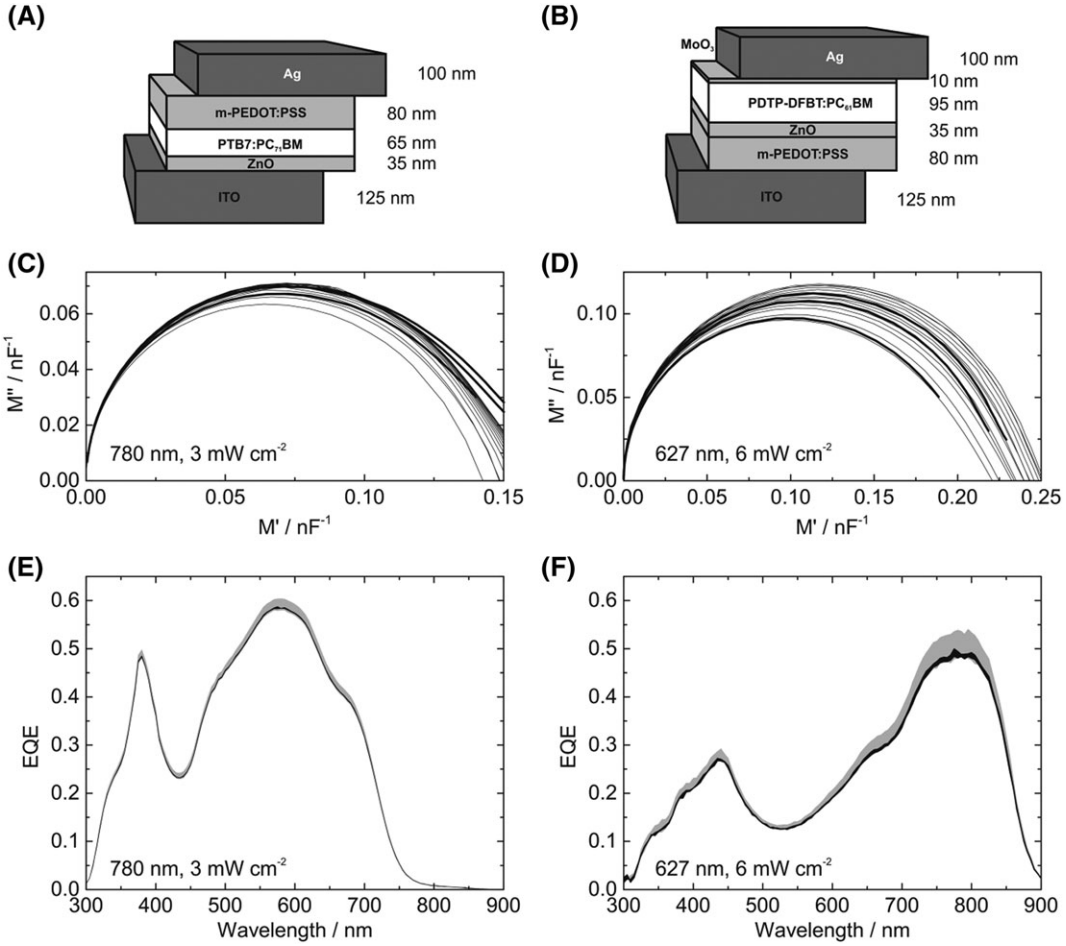

FIGURE 7 Left column: 780-nm LED bias light illumination; right column: 627-nm LED bias light illumination. A and B, Architectures of the single-junction reference devices. C and D, Voltage-dependent effective electric modulus (M_{eff}) plots of the tandem solar cell and electric modulus (M) plots of the reference devices. To determine the voltage applied to the current-limiting subcell, M plots of the reference devices (0 V, 0.25 V and 0.5 V) and M_{eff} plots of the tandem solar cell (0.5 to 1.2 V, step-width 0.05 V) are compared to calculate V_{bias} (see Tables 1 and 2). (E and F) Comparison of the tandem EQE measurements for different V_{tan}. The gray area shows the EQE span when V_{tan} is chosen anywhere from 0 V to the open-circuit voltage of the optically biased subcell under AM1.5 illumination. The span is significantly reduced if V_{tan} is selected from the voltage interval of V_{bias} that resulted from the impedance measurements (black area, see Table 3)

(Figure 7C,D, thin solid lines). As previously observed on the single-junction solar cells (Figure 2C,D), the measured electric modulus curves change with the applied voltage. In particular, the curve's diameter that corresponds to the capacitance of the current-limiting subcell decreases for increasing tandem voltages V_{tan}. Next, the electric moduli of the corresponding single-junction reference devices were measured at three different voltages (0, 0.25, and 0.50 V). Although the electric modulus of the solar cells is widely illumination independent, at very low intensities, we found that the electric modulus slightly diverges. In particular, measurement results in the dark are not comparable to measurement results under low illumination intensities. Therefore, applying a certain illumination intensity is useful to stabilize the working point and to avoid any ambient influences on the data. We recommend using the same light source for measuring the reference solar cells that was used for the tandem subcell saturation but at lower intensities - half the intensity should be a good initial choice. For the PDTP-DFBT:$PC_{61}BM$ reference solar cell, this corresponds to a 3.0 mW cm^{-2} illumination using the 627-nm LEDs. For the PTB7:$PC_{71}BM$ reference solar cell, in principle, a 780-nm LED illumination at 1.5 mW cm^{-2} would be recommended. But the latter case is more complex: The EQE onset (long-wavelength edge of the EQE spectrum) of the PTB7:$PC_{71}BM$ subcell is effectively shifted to 750 nm, which we attribute to the altered optical field in the tandem solar cell, whereas the onset of the reference solar cell can be found close to 780 nm (data not shown). This leads to a much weaker response of the PTB7:$PC_{71}BM$ subcell to the 780 nm bias light illumination compared to the reference solar cell. For such low absorption, the electric modulus response cannot be considered independent of the illumination intensity anymore. Hence, the number of absorbed photons in the tandem subcell has to match the total absorption in the reference device much better. Due to the shift of the EQE onset, a much lower intensity for illuminating the reference solar cell is required. In particular in this case, the comparison of the tandem electric modulus to the reference solar cell at various voltages, as discussed above, is necessary. Only under 0.4 mW cm^{-2} bias light illumination intensity, we found the electric moduli of the reference device comparable to the electric moduli of the tandem subcell within the applied voltage range.

By comparing the electric moduli of the tandem subcells and the corresponding reference devices (Figure 7C,D), voltages can be found where the electric moduli of the reference devices and the tandem

subcells match. The voltages derived under 780-nm bias light illumination are listed in Table 1, and the voltages derived under 627-nm bias light illumination are summarized in Table 2. Subtracting the reference solar cell voltage V_{ref} from the tandem voltage V_{tan} yields V_{bias} (using $V_{bias} = V_{tan} - V_{ref}$). Under 3.0 mW cm^{-2} of 780-nm LED bias illumination, an external voltage $V_{tan} = V_{bias}$ between 0.60 and 0.65 V has to be applied to the tandem solar cell to set the current-limiting subcell to short-circuit. When applying 6.0 mW cm^{-2} of 627-nm bias light illumination, a V_{tan} between 0.63 and 0.71 V is required. This is comparable to what was measured at the 3-terminal devices directly (780 nm, 3.0 mW cm^{-2}: 0.67 V; 627 nm, 6.0 mW cm^{-2}: 0.68 V). Accordingly, EQE measurements were performed at the estimated upper and lower limits of V_{tan} (780 nm, 3.0 mW cm^{-2}: 0.60 and 0.65 V; 627 nm, 6.0 mW cm^{-2}: 0.63 and 0.71 V). The resulting EQEs yield the black area in Figures 7E,F and correspond to the short-circuit current densities listed in Table 3. Notably, the accuracy has significantly improved compared to the common practice where any voltages between 0 V and the V_{oc} are applied (gray area in Figure 7E,F). From these EQEs, the short-circuit current densities J_{sc} of the subcells under irradiation of one sun (AM1.5 standard spectrum) can be calculated. For the PDTP-DFBT:PC$_{61}$BM subcell, the J_{sc} span (ie, the difference of the lower and the upper limit of the black area) is 0.15 mA cm^{-2} (<2%). For the PTB7:PC$_{71}$BM subcell, the J_{sc} span is only 0.03 mA cm^{-2}. For reference, using any bias voltage between 0 V and the V_{oc} of the current-limiting subcell leads to a J_{sc} span of 0.93 mA cm^{-2} for the PDTP-DFBT:PC$_{61}$BM subcell and to a J_{sc} span of 0.4 mA cm^{-2} for the PTB7:PC$_{71}$BM subcell. All data are summarized in Table 3.

The results also indicate a slightly mismatched photocurrent in both subcells, and hence, the PDTP-DFBT:PC$_{61}$BM subcell limits the tandem short-circuit current density. To determine the device efficiency according to the EQE results, in a first approximation, we adjusted the solar simulator to an intensity where the tandem solar cell exhibits a short-circuit current density of 9.0 mA cm^{-2}, which corresponds to the short-circuit current density of the current-limiting PDTP-DFBT:PC$_{61}$BM subcell and recorded the *J-V* curve (Figure 8). With an open-circuit voltage V_{oc} = 1.47 V and a fill factor *FF* = 60%, we obtain a PCE = 8.0%. We note that the EQEs of the subcells were

TABLE 1 Bias voltages extracted from the effective modulus plots of the PTB7:PC$_{71}$BM reference devices and the tandem solar cell under 780-nm LED bias light illumination

Device	Irradiance, mW cm^{-2}	Voltages, V		
Reference solar cell (V_{ref})[a]	0.4	0	0.25	0.50
Tandem subcell (V_{tan})	3.0	…[b]	0.90	1.10
Bias voltage (V_{bias})		…	0.65	0.60

The voltages are determined from matching curves in Figure 7C ($V_{ref} = V_{int}$). The difference between the tandem (V_{tan}) and the reference device voltages (V_{ref}) yields the bias voltage to be applied during external quantum efficiency measurement.

[a]Device architecture ITO/ZnO/PTB7:PC$_{71}$BM/m-PEDOT:PSS/Ag as depicted in Figure 7A.

[b]No matching tandem electric modulus plot observed due to only small variations for different applied voltages.

TABLE 2 Bias voltages extracted from the effective modulus plots of the PDTP-DFBT:PC$_{61}$BM reference device and the tandem solar cell under 627-nm LED bias light illumination

Device	Irradiance, mW cm^{-2}	Voltages, V		
Reference cell (V_{ref})[a]	3.0	0	0.25	0.50
Tandem subcell (V_{tan})	6.0	0.71	0.94	1.13
Bias voltage (V_{bias})		0.71	0.69	0.63

The data correspond to Figure 7D.

[a]Device architecture ITO/m-PEDOT:PSS/ZnO/PDTP-DFBT:PC$_{61}$BM/MoO$_3$/Ag as depicted in Figure 7B.

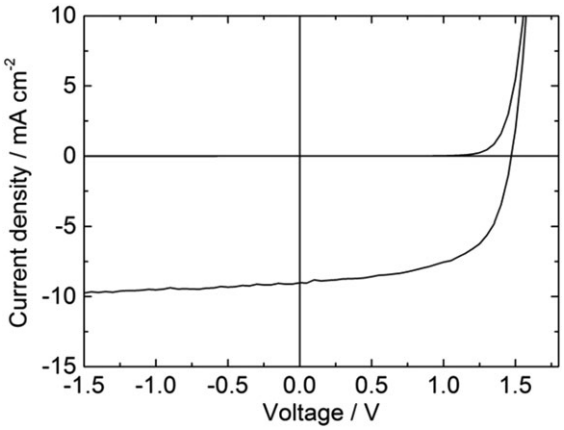

FIGURE 8 Current density-voltage curve of the PTB7:PC$_{71}$BM/PDTP-DFBT:PC$_{61}$BM tandem solar cell measured under illumination from a solar simulator. The illumination intensity was adjusted according to the current density of the current-limiting PDTP-DFBT:PC$_{61}$BM subcell as calculated from the external quantum efficiency measurements

TABLE 3 Overview of the external quantum efficiency (EQE) measurement parameters

Device	Bias Wavelength, nm	Irradiance, mW cm^{-2}	V_{tan}, V		J_{sc}, mA cm^{-2}		
			Min	Max	Max	Min	Span
PTB7:PC$_{71}$BM subcell	780	3.0	0	0.65	10.10	9.70	0.40
PDTP-DFBT:PC$_{61}$BM subcell	627	6.0	0	0.73	9.84	8.91	0.93
PTB7:PC$_{71}$BM subcell	780	3.0	0.60	0.65	9.79	9.76	0.03
PDTP-DFBT:PC$_{61}$BM subcell	627	6.0	0.63	0.71	9.09	8.94	0.15

The first two rows show the span of the short-circuit current density (J_{sc}) calculated from the EQE when the commonly used external tandem voltages (V_{tan}) of either 0 V or the open-circuit voltage of the subcell are applied. However, if the illumination intensities and the bias voltages (Table 1) were determined from the impedance measurements (rows 3 and 4), the span estimated as the difference between the maximum and minimum of the calculated J_{sc} is drastically reduced. The results also indicate a slightly mismatched photocurrent in both subcells, and hence, the J_{sc} of the tandem solar cell being limited to around 9.0 mA cm^{-2} by the PDTP-DFBT:PC$_{61}$BM subcell.

determined using a selective bias light intensity much lower than standard AM1.5 illumination. To further improve the measurement, the bias light illumination intensity must be increased, eg, by adding a spectrally broad bias light, which we deliberately omitted herein for clarity of this report. Furthermore, for an even more accurate measurement, the solar simulator has to be adjusted taking into account the spectral mismatch factor which can be calculated following established standard procedures.[12]

6 | CONCLUSION

This work proposes a reliable procedure to determine the minimum bias illumination intensity and the exact external voltage $V_{tan} = V_{bias}$ required for an accurate EQE measurement on subcells in tandem solar cells. It is based on observing voltage changes of the subcells by means of impedance spectroscopy. Graphically analyzing electric modulus curves, we found a method to predict both parameters. The minimum bias light illumination intensity that is required to saturate the optically biased subcell, can be determined from light intensity dependent impedance measurements by tracking the valley between the 2 semicircles of the tandem subcells in the electric modulus plot. In contrast to the estimation of the minimum bias illumination intensity from bias-light intensity dependent EQE measurements, this method is not affected by other intensity dependent processes. The bias voltage that is required to compensate the electric field introduced by the optically biased subcell can be determined by comparing electric modulus plots of the tandem subcells and of appropriate reference devices. Especially for organic tandem solar cells where high bias-light intensities are required and where the correct bias voltage often deviates from the open-circuit voltage of the optically biased subcell, this procedure can improve the measurement accuracy. We have deliberately exemplified the applicability of the measurement procedure to organic tandem solar cells, but it may be extended to other tandem solar cell architectures as well.

7 | SUGGESTED EQE AND PCE MEASUREMENT PROTOCOL FOR (ORGANIC) TANDEM SOLAR CELLS

To measure the performance of (organic) tandem solar cells and their subcells with higher precision in the future, we propose the following protocol. This protocol extends the ASTM E2236 standard which describes *Standard Test Methods for Measurement of Electrical Performance and Spectral Response of Nonconcentrator Multijunction Photovoltaic Cells and Modules*.[12] To perform all measurements under equal illumination conditions, a combined setup for EQE measurements and impedance measurements is required.

1. *Reference devices*: For each tandem subcell, fabricate a proper single-junction reference solar cell and measure the electric moduli of both reference devices under different illumination intensities. Proceed only, if the diameter of the electric modulus curves of both reference solar cells are illumination intensity independent.
2. *Tandem solar cell*: Replace the reference device in the measurement setup by the tandem solar cell.
3. *Selective bias light*: Choose a selective bias light with appropriate wavelength to saturate one of the subcells. Selective bias illuminations spectrally close to the absorption onset of one of the subcells cell should be avoided.
4. *Additional bias light*: Since the EQE of the current-limiting subcell may be illumination dependent, apply additional bias illumination to generate a total photocurrent about equal to the photocurrent expected under AM1.5 illumination. Such bias light can, for example be applied from a solar simulator. However, the illumination intensity from the selective bias light should be higher for generating a sufficient charge carrier excess.
5. *Voltage saturation*: Test the internal voltage saturation by measuring the electric modulus of the tandem solar cell as a function of the selective bias light illumination intensity. If the electric modulus remains stable for further increasing intensities, internal voltage saturation is fulfilled and the intensity of the selective bias light illumination is sufficiently high. If the electric modulus cannot be stabilized, choose another selective bias light and return to step 3.
6. *Electric modulus* (*tandem solar cell*): Using the determined illumination intensities, measure the voltage-dependent electric modulus of the tandem solar cell. Calculate and plot $M_{corr} = j\omega C_0(Z - R_{s,\ eff})$ (Equation 9). $R_{s,eff}$ can be derived from the position of the valley in the electric modulus curve using $R_{s,eff} = \frac{M_v''}{\omega_v}$ (Equation 13 and Figure 5).
7. *Reduced light intensity for reference device measurement*: Replace the tandem solar cell by the corresponding reference device. Reduce the illumination intensity to account for the higher absorption of the reference device compared to the tandem subcell. A rough estimation is sufficient since the electric modulus is illumination independent (step 1).
8. *Electric modulus* (*reference solar cell*): Measure the voltage-dependent electric modulus of the reference solar cell and compare the data to the tandem solar cell data gained in step 6. For matching electric modulus curves, the voltage applied to the reference device ($V_{ref} = V_{int}$) can be subtracted from the voltage applied to the tandem device (V_{tan}) to calculate the bias voltage ($V_{bias} = V_{tan} - V_{int}$).
9. *Subcell EQE 1*: Again, place the tandem solar cell into the measurement setup and apply the bias light (intensity, wavelength) and bias voltage previously determined in steps 5 and 8, respectively. Measure the spectral response of the current-limiting subcell. Calculate the EQE of the subcell.
10. *Subcell EQE 2*: Repeat steps 2 to 9 to measure the other subcell.

Proceed with electrical performance measurements as described in ASTM standard[12] E2236. This includes measurement of the *J-V* curve of the tandem solar cell and spectral mismatch factor calculation. Thereupon, the *J-V* curve under AM1.5 standard irradiation and the resulting PCE of the tandem device can be calculated.

8 | EXPERIMENTAL

8.1 | Device fabrication

The 2-terminal tandem solar cells were fabricated according to the device architecture that is depicted in Figure 3A. Therefore, ITO coated glass sheets ($R_{\square}$ = 13 Ω sq^{-1}) were structured with hydrochloric acid and subsequently cleaned in an ultrasonic bath using acetone (10 min) and 2-propanol (10 min). For device fabrication, all substrates were transferred into a glovebox with nitrogen atmosphere. Zinc oxide nanoparticles were spin coated from 2-propanol dispersion (1% *w*/w, Nanograde Ltd, 4000 rpm, 30 s) and dried (80°C, 10 min). The bottom absorber blend comprising poly[[4,8-bis[(2-ethylhexyl)oxy]benzo[1,2-*b*:4,5-*b*′]dithiophene-2,6-diyl][3-fluoro-2-[(2-ethylhexyl)carbonyl]thieno[3,4-*b*]thiophenediyl]] (PTB7, 1-Material Inc, M_w = 125 kg mol^{-1}, $Đ_M$ = 2.5) and [6,6]-phenyl C_{71}-butyric acid methyl ester ($PC_{71}BM$, Solenne B.V.) was dissolved in chlorobenzene (2:3 w/w, 23 g L^{-1}). After adding the co-solvent diiodooctane (4% *v*/v), the PTB7:$PC_{71}BM$ blend was spin coated from warm solution (60°C, 2000 rpm, 60 s) and dried (60°C, 20 min). The recombination zone of the tandem solar cell comprised poly[3,4-ethylenedioxythiophene]:poly[4-styrenesulfonate] (PEDOT:PSS, formulation Clevios HTL Solar, Heraeus Deutschland GmbH & Co KG) and ZnO. PEDOT:PSS was modified (m-PEDOT:PSS) by adding sodium polystyrenesulfonate solution (100 g L^{-1} in deionized water) (25:1 v/v) to improve the solvent barrier properties of the intermediate recombination zone as reported earlier.[38] Then m-PEDOT:PSS was spin coated atop the bottom absorber layer (4000 rpm, 40 s) and dried (80°C, 10 min). ZnO was deposited as described above. The top absorber blend comprising poly[[2,7-(5,5-bis-(3,7-dimethyloctyl)-5H-dithieno[3,2-*b*:2′,3′-*d*]pyran)-*alt*-4,7-(5,6-difluoro-2,1,3-benzothiadiazole)]] (PDTP-DFBT, 1-Material Inc, M_w = 37 kg mol^{-1}, $Đ_M$ = 2.4) and [6,6]-phenyl C_{61}-butyric acid methyl ester ($PC_{61}BM$, Solenne B.V.) was dissolved in *o*-xylene (2:3 w/w, 25 g L^{-1}). After adding the co-solvent *p*-anisaldehyde (1% v/v), the PDTP-DFBT:$PC_{61}BM$ blend was spin coated (solution at 60°C, 1200 rpm, 60 s) and dried (60°C, 10 min) as reported earlier.[39] The molybdenum oxide/silver counter electrodes were thermally evaporated in high vacuum (10^{-7} mbar) through an aligned shadow mask. The photoactive device area was defined by the cross section of the electrodes (3.0 × 3.5 mm^2).

The 3-terminal tandem solar cells were fabricated according to the device architecture in Figure 1A. Therefore, we followed the same recipe, but the m-PEDOT:PSS single layer was replaced by a bilayer of conductive PEDOT:PSS (c-PEDOT:PSS, Clevios F HC Solar, Heraeus Deutschland GmbH & Co KG) and m-PEDOT:PSS (both diluted with deionized water 2:1 v/v, 4000 rpm, 40 s). The total thickness of the bilayer was equal to the thickness of the m-PEDOT:PSS layer in the 2-terminal tandem solar cell to yield equal optoelectronic properties in both recombination zones.[7] The c-PEDOT:PSS layer was laterally structured by a lift-off process using a sticky tape as reported earlier.[7] Both PEDOT:PSS layers were dried (80°C, 10 min).

For reference, we fabricated ITO/ZnO/PTB7:$PC_{71}BM$/m-PEDOT:PSS/Ag and ITO/m-PEDOT:PSS/ZnO/PDTP-DFBT:$PC_{61}BM$/MoO_3/Ag single junction solar cells (Figure 7A,B), following the layer recipes above.

8.2 | Thickness measurements

All layer thicknesses were measured on single layers that were coated separately on glass sheets, using a profiler (Dektak XT, Bruker).

8.3 | Device encapsulation

All devices were encapsulated using an UV-curing adhesive (KATIOBOND OB642, DELO Industrial Adhesives) to enhance the device stability during impedance spectroscopy measurements under ambient conditions.

8.4 | Optical simulations

Optical simulations used the transfer matrix method.[40] All complex refractive indices were determined by spectroscopic ellipsometry (WVASE, LOT Woolam) from single layers on glass substrates. The LED spectra used in the simulations were measured by a fiber optic spectrometer (EPP2000, StellarNet).

8.5 | EQE measurements

The EQE measurements were performed under inert conditions in a glovebox using a customized setup. The chopped monochromatic probe light (473.3 Hz) was generated by a high-pressure xenon plasma lamp (450 W, LSH601, LOT Oriel) attached to a Czerny-Turner monochromator (Omni-λ300, LOT Oriel) and a filter wheel to suppress higher order wavelengths (MSZ3122, LOT Oriel). The short-circuit current of the devices generated by the monochromatic probe light was measured using a transimpedance amplifier (DLPCA-S, Femto Messtechnik GmbH) and a lock-in amplifier (eLockIn 203, Anfatec Instruments AG) synchronized to the optical chopper (C-995, Terahertz Technologies Inc). During the measurement, the intensity of the chopped monochromatic probe light was monitored using a photo diode (K1713-09, Hamamatsu). Its currents were measured by an additional transimpedance amplifier (DLPCA-S, Femto Messtechnik GmbH). Prior to the EQE measurements, the spectral response of the monitor diode was determined using a calibrated reference silicon photodiode (SM1PD2A-CAL, Thorlabs). For bias illumination with 780 nm, a ring of LEDs (25× LED780E, Thorlabs GmbH), and for bias illumination with 627 nm, an illuminator kit (LDC627, Metrohm Autolab B.V.) with 3 LEDs were installed. Their spectra are depicted in Figure 4G,H. Their intensities were adjusted using a silicon photodiode (SM1PD2A-CAL, Thorlabs) connected to a source measure unit (Model 238, Keithley).

8.6 | Impedance measurements

For impedance measurements, the potentiostat PGSTAT302N and the impedance module FRA32M (Metrohm Autolab B.V.) were used. All impedance measurements herein were performed at a voltage amplitude of 10 mV. For illumination, the same LED light sources as used for the EQE measurements were installed on an optical bench. The illumination intensity was measured using a calibrated silicon photodiode (AUT.LED.PHDIODE, Metrohm Autolab B.V.). All measurements were performed with 4-wire connection. The influence of the

impedance of the wires was corrected by the software from an initial measurement with the wires detached from the samples.

8.7 | Current density-voltage (*J-V*) measurements

All electrical measurements under LED illumination were performed in ambient atmosphere using the potentiostat (see above). To avoid any influences from the resistance of the intermediate contact, the subcells' *J-V* curves of the 3-terminal tandem solar cells were measured in 4-wire sensing mode as follows: The force wires were connected to the outer tandem solar cell contacts (2-terminal mode); the sense wires were connected to one of the subcells using the intermediate contact and the respective outer contact. The *J-V* curves of the tandem solar cells under simulated sunlight (300 W, M-91160, Newport) were performed under inert conditions in a glovebox using a source measure unit (Model 238, Keithley).

ACKNOWLEDGEMENTS

We acknowledge the German Federal Ministry of Education and Research (BMBF) for funding under contract 03EK3504 (project TAURUS). We acknowledge Nanograde Inc for providing zinc oxide nanoparticle dispersions, 1-Material Inc for providing different batches of the absorber polymer, PDTP-DFBT for evaluation, and DELO Industrial Adhesives for supplying samples of different UV-curing adhesives for encapsulation. We thank Christian Sprau, Dino Klotz, and Sabrina Jüchter for fruitful discussions.

ORCID

Alexander Colsmann http://orcid.org/0000-0001-9221-9357

REFERENCES

1. Zimmermann E, Ehrenreich P, Pfadler T, Dorman JA, Weickert J, Schmidt-Mende L. Erroneous efficiency reports harm organic solar cell research. *Nature Photon*. 2014;8:669. https://doi.org/10.1038/nphoton.2014.210
2. Timmreck R, Meyer T, Gilot J, et al. Characterization of tandem organic solar cells. *Nature Photon*. 2015;9:478. https://doi.org/10.1038/nphoton.2015.124
3. ASTM Standard G173, 2012, "*Reference solar spectral irradiances: Direct normal and hemispherical on 37° tilted surface*," ASTM International, West Conshohocken, PA, 2012, doi: https://doi.org/10.1520/G0173, www.astm.org.
4. ASTM Standard E1021, 2015, "*Standard test method for spectral responsivity measurements of photovoltaic devices*," ASTM International, West Conshohocken, PA, 2015, doi: https://doi.org/10.1520/E0973, www.astm.org.
5. Wehenkel DJ, Hendriks KH, Wienk MM, Janssen RAJ. The effect of bias light on the spectral responsivity of organic solar cells. *Org Electron*. 2012;13:3284. https://doi.org/10.1016/j.orgel.2012.09.040
6. Shrotriya V, Li G, Yao Y, Moriarty T, Emery K, Yang Y. Accurate measurement and characterization of organic solar cells. *Adv Funct Mater*. 2006;16:2016. https://doi.org/10.1002/adfm.200600489
7. Bahro D, Koppitz M, Mertens A, Glaser K, Mescher J, Colsmann A. Understanding the external quantum efficiency of organic homo-tandem solar cells utilizing a three-terminal device architecture. *Adv Energy Mater*. 2015;5:1501019. https://doi.org/10.1002/aenm.201501019
8. Burdick J, Glatfelter T. Spectral response and I–V measurements of tandem amorphous-silicon alloy solar cells. *Solar Cells*. 1986;18:301. https://doi.org/10.1016/0379-6787(86)90129-8
9. Kurtz SR, Emery K, Olson JM. Methods for analysis of two-functional, two-terminal photovoltaic devices. Proc. of the First World Conference on Photovoltaic. *Energy Conversion*. 1994;1733. https://doi.org/10.1109/WCPEC.1994.520553
10. Gilot J, Wienk MM, Janssen RAJ. Measuring the external quantum efficiency of two-terminal polymer tandem solar cells. *Adv Funct Mater*. 2010;20:3904. https://doi.org/10.1002/adfm.201001167
11. Chen CC, Bae SH, Chang WH, et al. Perovskite/polymer monolithic hybrid tandem solar cells utilizing a low-temperature, full solution process. *Mater Horiz*. 2015;2:203. https://doi.org/10.1039/C4MH00237G
12. ASTM Standard E2236, 2015, "*Standard test methods for measurement of electrical performance and spectral response of nonconcentrator multijunction photovoltaic cells and modules1*," ASTM International, West Conshohocken, PA, 2015, doi: https://doi.org/10.1520/E0973, www.astm.org.
13. Lee J, Kang H, Kong J, Lee K. A depletion-free, ionic, self-assembled recombination layer for tandem polymer solar cells. *Adv Energy Mater*. 2014;4:1301226. https://doi.org/10.1002/aenm.201301226
14. Li N, Brabec CJ. Air-processed polymer tandem solar cells with power conversion efficiency exceeding 10%. *Energ Environ Sci*. 2015;8:2902. https://doi.org/10.1039/C5EE02145F
15. Li K, Li Z, Feng K, Xu X, Wang L, Peng Q. Development of large band-gap conjugated copolymers for efficient regular single and tandem organic solar cells. *J Am Chem Soc*. 2013;135:13549. https://doi.org/10.1021/ja406220a
16. Vasilopoulou M, Polydorou E, Douvas AM, Palilis LC, Kennouc S, Argitisa P. Annealing-free highly crystalline solution-processed molecular metal oxides for efficient single-junction and tandem polymer solar cells. *Energ Environ Sci*. 2015;8:2448. https://doi.org/10.1039/C5EE01116G
17. You J, Dou L, Yoshimura K, et al. A polymer tandem solar cell with 10.6% power conversion efficiency. *Nat Commun*. 2013;4:1446. https://doi.org/10.1038/ncomms2411
18. Riede M, Uhrich C, Widmer J, et al. Efficient organic tandem solar cells based on small molecules. *Adv Funct Mater*. 2011;21:3019. https://doi.org/10.1002/adfm.201002760
19. Dou L, You J, Yang J, et al. Tandem polymer solar cells featuring a spectrally matched low-bandgap polymer. *Nature Photon*. 2012;6:180. https://doi.org/10.1038/nphoton.2011.356
20. Timmreck R, Leo K, Riede M. Characterization of tandem organic solar cells comprising subcells of identical absorber material. *Prog Photovolt: Res Appl*. 2015;23:1353. https://doi.org/10.1002/pip.2541
21. Si FT, Isabella O, Zeman M. Artifact interpretation of spectral response measurements on two-terminal multijunction solar cells. *Adv Energy Mater*. 2017;7:1601930. https://doi.org/10.1002/aenm.201601930
22. Bahro D, Koppitz M, Colsmann A. Tandem organic solar cells revisited. *Nature Photon*. 2016;10:354. https://doi.org/10.1038/nphoton.2016.96
23. Macdonald JR, Johnson WB. In: Barsoukov E, Macdonald JR, eds. *Impedance spectroscopy theory, experiment, and applications, second edition*. Hoboken, New Jersey: John Wiley & Sons, Inc.; 2005. ISBN:0-471-64749-7.
24. Mitul AF, Mohammad L, Venkatesan S, et al. Low temperature efficient interconnecting layer for tandem polymer solar cells. *Nano Energy*. 2015;11:56. https://doi.org/10.1016/j.nanoen.2014.09.026
25. Arredondo B, Martín-López MB, Romero B, Vergaz R, Romero-Gomez P, Martorell J. Monitoring degradation mechanisms in PTB7:$PC_{71}BM$ photovoltaic cells by means of impedance spectroscopy. *Sol Energy Mater Sol Cells*. 2016;144:422-428. https://doi.org/10.1016/j.solmat.2015.09.050
26. Fabregat-Santiago F, Garcia-Belmonte G, Mora-Seróa I, Bisquert J. Characterization of nanostructured hybrid and organic solar cells by impedance spectroscopy. *Phys Chem Chem Phys*. 2011;13:9083. https://doi.org/10.1039/C0CP02249G

27. Guerrero A, Montcada NF, Ajuria J, et al. Charge carrier transport and contact selectivity limit the operation of PTB7-based organic solar cells of varying active layer thickness. *J Mater Chem A*. 2013;1:12345-12354. https://doi.org/10.1039/C3TA12358H

28. Garcia-Belmonte G, Boix PP, Bisquert J, Sessolo M, Bolink HJ. Simultaneous determination of carrier lifetime and electron density-of-states in P3HT:PCBM organic solar cells under illumination by impedance spectroscopy. *Sol Energy Mater Sol Cells*. 2010;94:366. https://doi.org/10.1016/j.solmat.2009.10.015

29. Bisquert J, Fabregat-Santiago F, Mora-Seró I, Garcia-Belmonte G, Barea EM, Palomares E. A review of recent results on electrochemical determination of the density of electronic states of nanostructured metal-oxide semiconductors and organic hole conductors Inorg. *Chim Acta*. 2008;361:684. https://doi.org/10.1016/j.ica.2007.05.032

30. Cole KS, Cole RH. Dispersion and absorption in dielectrics I. Alternating Current Characteristics. *J Chem Phys*. 1941;9:341. https://doi.org/10.1063/1.1750906

31. McCrum NG, Read BE, Williams G. *Anelastic and dielectric effects in polymeric solids*. London: Wiley; 1967.

32. Glatthaar M, Riede M, Keegan N, et al. Efficiency limiting factors of organic bulk heterojunction solar cells identified by electrical impedance spectroscopy. *Sol Energy Mater Sol Cells*. 2007;91:390. https://doi.org/10.1016/j.solmat.2006.10.020

33. Bisquert J, Mora-Sero I, Fabregat-Santiago F. Diffusion–recombination impedance model for solar cells with disorder and nonlinear recombination. *ChemElectroChem*. 2014;1:289. https://doi.org/10.1002/celc.201300091

34. Leever BJ, Bailey CA, Marks TJ, Hersam MC, Durstock MF. In situ characterization of lifetime and morphology in operating bulk heterojunction organic photovoltaic devices by impedance spectroscopy. *Adv Energy Mater*. 2012;2:120. https://doi.org/10.1002/aenm.201100357

35. Garcia-Belmonte G, Guerrero A, Bisquert J. Elucidating operating modes of bulk-heterojunction solar cells from impedance spectroscopy analysis. *J Phys Chem Lett*. 2013;4:877. https://doi.org/10.1021/jz302064z

36. Liang Y, Xu Z, Xia J, et al. For the bright future—Bulk heterojunction polymer solar cells with power conversion efficiency of 7.4%. *Adv Mater*. 2010;22:E135. https://doi.org/10.1002/adma.200903528

37. You J, Chen CC, Hong Z, et al. 10.2% Power conversion efficiency polymer tandem solar cells consisting of two identical sub-cells. *Adv Mater*. 2013;25:3973. https://doi.org/10.1002/adma.201300964

38. Yang J, Zhu R, Hong Z, et al. A robust inter-connecting layer for achieving high performance tandem polymer solar cells. *Adv Mater*. 2011;23:3465. https://doi.org/10.1002/adma.201100221

39. Sprau C, Buss F, Wagner M, et al. Highly efficient polymer solar cells cast from non-halogenated xylene/anisaldehyde solution. *Energ Environ Sci*. 2015;8:2744. https://doi.org/10.1039/C5EE01917F

40. Christ NS, Kettlitz SW, Valouch S, et al. Nanosecond response of organic solar cells and photodetectors. *J Appl Phys*. 2009;105:104513. https://doi.org/10.1063/1.3130399

SUPPORTING INFORMATION

Additional Supporting Information may be found online in the supporting information tab for this article.

How to cite this article: Bahro D, Wilck M, Mertens A, Ebenhoch B, von Hauff E, Colsmann A. Organic tandem solar cells: How impedance analyses can improve the quality of external quantum efficiency measurements. *Prog Photovolt Res Appl*. 2018;26:763–777. https://doi.org/10.1002/pip.3015